

East African climate change and orbital forcing during the last 175 kyr BP

Martin H. Trauth^{a,*}, Alan L. Deino^b, Andreas G.N. Bergner^a,
Manfred R. Strecker^a

^a *Institut für Geowissenschaften, Universität Potsdam, P.O. Box 601553, 14415 Potsdam, Germany*

^b *Berkeley Geochronology Center, 245 Ridge Road, Berkeley, CA 94709, USA*

Received 28 June 2002; received in revised form 31 October 2002; accepted 12 November 2002

Abstract

Variations in the temporal and spatial distribution of solar radiation caused by orbital changes provide a partial explanation for the observed long-term fluctuations in African lake levels. The understanding of such relationships is essential for designing climate-prediction models for the tropics. Our assessment of the nature and timing of East African climate change is based on lake-level fluctuations of Lake Naivasha in the Central Kenya Rift (0°55'S 36°20'E), inferred from sediment characteristics, diatoms, authigenic mineral assemblages and 17 single-crystal ⁴⁰Ar/³⁹Ar age determinations. Assuming that these fluctuations reflect climate changes, the Lake Naivasha record demonstrates that periods of increased humidity in East Africa mainly followed maximum equatorial solar radiation in March or September. Interestingly, the most dramatic change in the Naivasha Basin occurred as early as 146 kyr BP and the highest lake level was recorded at about 139–133 kyr BP. This is consistent with other well-dated low-latitude climate records, but does not correspond to peaks in Northern Hemisphere summer insolation as the trigger for the ice-age cycles. The Naivasha record therefore provides evidence for low-latitude forcing of the ice-age climate cycles.

© 2002 Elsevier Science B.V. All rights reserved.

Keywords: Rift; Quaternary; lake sediments; paleoclimate; Ar-40/Ar-39 dating; geochronology

1. Introduction

Tropical African climate is mainly controlled by the strength of the African–Asian monsoonal circulation and the position and seasonal migration of the Intertropical Convergence Zone

(ITCZ) (Fig. 1a). The zone of maximum rainfall follows the latitudinal position of the overhead sun with a time lag of about 4–6 weeks. This results in one rainy season in most of the northern and southern sectors of the continent, whereas the annual cycle of rainfall in equatorial East Africa is bimodal with rainy seasons in April–May and October–November. During the Pleistocene, African climatic changes on time scales of thousands of years were apparently paced by periodic (23–19 kyr) variations in insolation resulting from

* Corresponding author. Tel.: +49-331-977-2288;
Fax: +49-331-977-2087.
E-mail address: trauth@geo.uni-potsdam.de (M.H. Trauth).

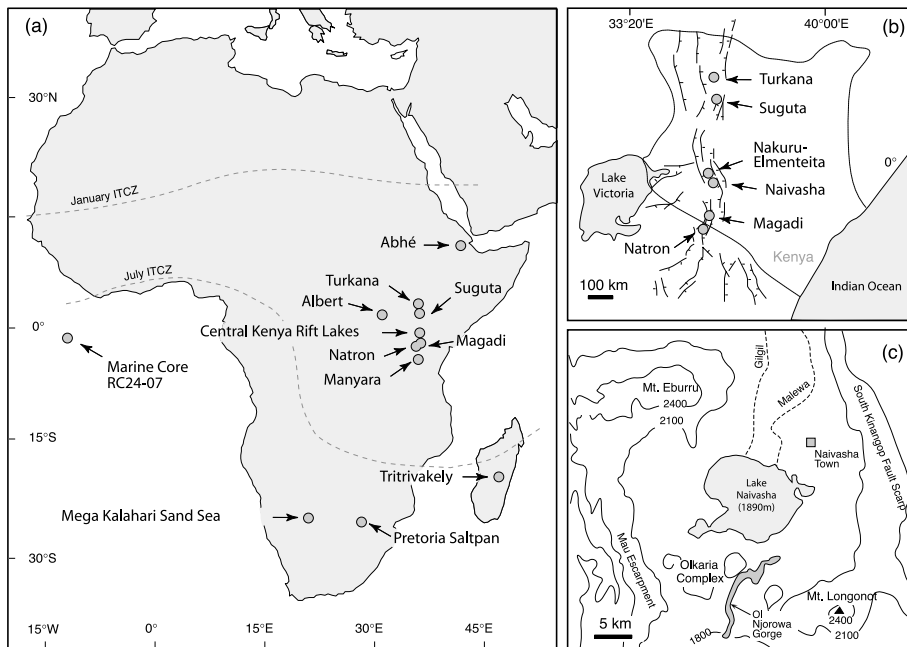


Fig. 1. (a) Location of sites mentioned in the text. (b) Kenya Rift showing Lake Turkana, paleo-Lake Suguta, Lake Naivasha and Lake Nakuru-Elmenteita and Lake Magadi. (c) Naivasha Basin showing location of the Ol Njorowa Gorge, the Olkaria, Mt. Eburru and Mt. Longonot volcanic complexes. The Gilgil and Malewa rivers are the main water sources of modern Lake Naivasha.

Earth's orbital precession [1–3]. Due to the geometry of precession, changes in summer solar radiation are in antiphase between hemispheres, causing maximum monsoonal circulation and moister climate every 23–19 kyr in North and South Africa [4–7]. In contrast, periods of increased humidity in equatorial East Africa occurred at 10–11 kyr intervals following maximum equatorial insolation in March and September [8].

The timing of climate change in Africa during the last two glacial–interglacial cycles is still poorly known. This is partly due to the fact that few paleoclimate chronologies extending back to ~200 kyr are available. These records are usually well-dated for the last ~40 kyr but uncontrolled in the older parts, mainly because of the temporal limitations of the radiocarbon method [6,9,10]. Few records provide some evidence for a period of high lake levels and increased humidity at ~135 kyr BP, well before the intensification of the monsoon system after the penultimate glacial [11–13].

Recently, high-quality chronologies of tropical

climate have become particularly important in the discussion of a tropical forcing of deglaciation [14,15]. The key argument of this hypothesis is that tropical sea-surface temperatures (SSTs) lead high-latitude Northern Hemisphere ice volumes by several thousand years [16,17]. A tropical forcing of deglaciation could also help explain why ice ages occur in both hemispheres simultaneously although the changes in solar irradiance from orbital variations have opposite effects in the north and south [18]. However, these assessments are based on marine records, which are often difficult to date beyond the radiocarbon time scale.

Here, we present a precisely dated high-resolution lacustrine sequence of climate-induced hydrological changes from the closed Naivasha Basin (Central Kenya Rift) extending back to 176 kyr BP (Fig. 1b). A first compilation of the sediment characteristics and $^{40}\text{Ar}/^{39}\text{Ar}$ ages has been published in [8] and [19]. We present: (a) a more detailed description of the sedimentary sequence, (b) detailed statistical analysis of the geochronological information, and (c) a discussion of the timing

of the environmental changes during the last two glacial–interglacial cycles (marine isotope stages (MIS) 6–1). Our data provide important insights into tropical climate change and the role of the tropics in global climate change.

2. Setting

The present climate patterns in East Africa include several major air streams and convergence zones, superimposed upon regional factors associated with topography, large lakes, and maritime influence [20,21]. Regional wind and pressure patterns include the Congo air stream with westerly and southwesterly air flow, as well as the NE and SE monsoons. In contrast to the Asian SW monsoon, both monsoons over East Africa are relatively dry. In contrast, the Congo air stream is humid and associated with rainfall. These major air streams are separated by the Intertropical Convergence Zone (ITCZ) and the Congo Air Boundary. Rainfall in East Africa is mainly linked to the passage of the ITCZ causing a strongly bimodal annual cycle [21]. The period during April–May is considered to be the ‘long rains’ while the October–November period is called the ‘short rains’, following the latitudinal position of the overhead sun with a time lag of about 4–6 weeks. Fluctuations in the intensity of precipitation are linked to E–W adjustments in the zonal Walker circulation associated with the El Niño/Southern Oscillation (ENSO), but these may be more directly a response to SST variations in the Indian and Atlantic Oceans, which in turn are modulated by ENSO [21].

Located at 1890 m above sea level, Lake Naivasha is the highest lake in the Central Kenya Rift (0°55′S 36°20′E) (Fig. 1c). To the west the Naivasha Basin is bounded by east-dipping normal faults of the Mau Escarpment and by Mt. Eburru volcano; to the east the basin is bordered by west-dipping faults that separate the intrarift Kinangop Plateau from the eastern rift shoulder. To the north the basin is also limited by normal fault scarps, whereas the southern boundary comprises the trachytic Mt. Longonot volcano and the rhyolitic Olkaria Volcanic Complex (Fig.

1). The history of the Naivasha Basin began at about 320 kyr BP, when lava flows at Olkaria closed the southern basin outlet between the flanks of the 400 kyr old Mt. Longonot and the Mau Escarpment [22,23]. However, stratigraphical relations in the Ol Njorowa Gorge in the transition between the Olkaria Volcanic Complex and Mt. Longonot show that a large lake did not exist before ~146 kyr BP [8].

The majority of the volcanic units at Olkaria are younger than 20 kyr [23] and cover the predominantly lacustrine section exposed within the Ol Njorowa Gorge (Fig. 1). The gorge is the site of an outlet of a Holocene lake and was cut by headward erosion [24]. The lacustrine succession is 60 m thick and unconformably overlies the oldest rhyolitic lava flows and pyroclastics of the Olkaria Volcanic Complex [8,19] (Fig. 2). The deposits in the gorge are mainly yellow to buff waterlaid tuffs with altered lapilli. Diatomite and laminated siltstone are also common, as are intercalations of coarse clastic fluvial sediments and pyroclastic deposits indicating intermittent subaerial conditions. Except for major erosional unconformities at the top and base of the section, the lake sediment sequence is conformable. The base of the profile at 1840 m is 50 m below the present lake level. No sediments of similar age were found in the Naivasha Basin due to the lack of exposure [25].

Modern Lake Naivasha contains ~0.85 km³ of water over an area of about 170 km². Around 12% of the lake surface is covered by papyrus swamps. Whereas most of the Kenya Rift lakes such as Lake Elmenteita (1776 m) and Lake Nakuru (1758 m) are highly alkaline, Lake Naivasha is fresh and has a relatively low pH of ~8.1 [26]. Since the lake area receives only 600 mm yr⁻¹ of rain and potential evapotranspiration is about 1800 mm yr⁻¹ [23], this is most likely related to significant southward and northward groundwater seepage combined with a recharge by the Malewa and Gilgil rivers [22,26]. These two streams drain a large catchment area of 3200 km², which includes areas of high elevation on the eastern rift shoulder (i.e. the Kinangop Plateau and the 4400 m high Aberdare Range, where rainfall exceeds 1750 mm yr⁻¹ [23,27,28]) (Fig. 1c).

3. Methods

3.1. $^{40}\text{Ar}/^{39}\text{Ar}$ geochronology

We sampled a 60 m thick sedimentary and pyroclastic sequence in the Ol Njorowa Gorge, which was incised and exposed after the last lake-level highstand at around 10–6 kyr BP [24]. Anorthoclase and sanidine phenocryst concentrates from 16 tuff beds (ignimbrites, air-fall tuffs and reworked tuffs), and one lava flow were dated by the laser-fusion $^{40}\text{Ar}/^{39}\text{Ar}$ method (Figs. 2 and 3). The sampled units ranged stratigraphically from comenditic lava at the base of the volcanoclastic section in the Njorowa Gorge, to the prominent yellow tuffs forming the top of the section. Where feasible, phenocrysts were separated from hand-picked pumice lapilli.

Two variants of the laser-heat $^{40}\text{Ar}/^{39}\text{Ar}$ method were employed. The first is the ‘total-fusion’ technique (TF), in which individual crystals or small populations of grains (three to eight crystals) are fused in a pseudo two-step sequence. The first ‘step’, which is not analyzed, is a low-power outgassing of the grain surface using a defocused beam, primarily to strip away much of the adhering atmospheric argon. The second step consists of a rapid heating of the sample to fusion using a focused laser beam. Ar released by this step is analyzed in a magnetic-sector noble gas mass spectrometer to produce a date. Both Ar-ion and CO_2 lasers have been used as heating devices in this study. The second variant of the laser-heating $^{40}\text{Ar}/^{39}\text{Ar}$ method involves incremental heating and analysis of the 25–75 mg of sample at progressively higher power levels using a defocused CO_2 laser (IH technique). In this arrangement, the laser beam is passed through a special integrator lens to produce a square, 6×6 mm beam at the focal point, with a nominally uniform energy profile [29].

Samples were irradiated in the Cd-lined CLICIT facility of the University of Oregon TRIGA reactor for 30–45 min in two batches. Sanidine from the Fish Canyon Tuff of Colorado (28.02 Ma) was used as a flux monitor [30]. Additional details of the analytical technique can be found in [31,32]. To facilitate comparison of dating results,

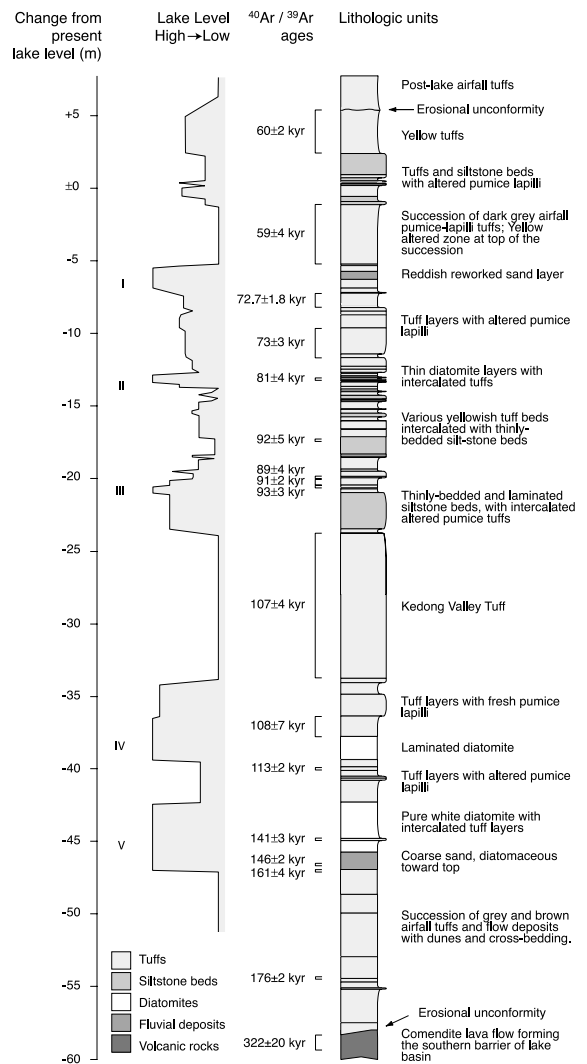


Fig. 2. Sediment profile of Ol Njorowa Gorge showing major lithologic units, $^{40}\text{Ar}/^{39}\text{Ar}$ ages and inferred lake-level fluctuations based on diagenetic mineral phases and diatomites.

^{14}C ages were converted to calendar ages as published in Radiocarbon 40, no. 3 (1998).

3.2. Reconstruction of lake-level fluctuations

The paleoecology of the basin was reconstructed using authigenic mineral phases (e.g. chabazite, clinoptilolite and analcime) [33–37] and siliceous algae (diatom) assemblages [38]. Bulk mineralogy was obtained from X-ray diffraction

using standard techniques. Silicic pyroclastic deposits in the profile allow an evaluation of lake alkalinity by means of the degree of alteration of volcanic glass and the presence of authigenic silicates. Authigenic silicates such as zeolites and potassium feldspar are common in ephemeral water bodies in arid or semiarid regions where high pH conditions result from concentration of sodium carbonate–bicarbonate due to evapotranspiration [33–37]. Similar to other lacustrine environments with alternating phases of water chemistry, vertical variations of authigenic mineral phases in the Naivasha sediment sequence thus define lake-level fluctuations and alkalinity changes through time [8,19]. Freshwater phases are characterized by diatomite, unaltered volcanic glass and absence of authigenic silicates. In contrast, silicic glass with perlitic cracks, glass shards with montmorillonite rims, occasional chabazite and phillipsite represent the transition to alkaline conditions with a pH of about 9. Even higher alkalinity results in the formation of clinoptilolite, and extremely alkaline pore waters lead to the precipitation of analcime [8,19].

4. Results

4.1. $^{40}\text{Ar}/^{39}\text{Ar}$ geochronology

Table 1a–c summarizes analytical data for the $^{40}\text{Ar}/^{39}\text{Ar}$ incremental-heating analyses; Fig. 3a graphically portrays these experiments as cumulative % ^{39}Ar release spectra. Most samples exhibit a broad plateau encompassing more than 90% of the total ^{39}Ar released, with the exception of sample NJOR94-8, in which the plateau covered only 65% of the gas release, and sample NJOR94-7, which failed to generate a plateau (defined in Table 1a–c). Plateau ages are indistinguishable from integrated ages, the age generated when all steps are mathematically recombined to simulate a total-fusion experiment. Inverse isochron analyses ($^{36}\text{Ar}/^{40}\text{Ar}$ vs. $^{39}\text{Ar}/^{40}\text{Ar}$, corrected for decay, mass spectrometer discrimination, and isotopic interferences) of the plateau regions yield ages which agree with the plateau ages (Table 1a). The ‘trapped’ $^{40}\text{Ar}/^{36}\text{Ar}$ component derived from

the inverse isochron analysis yields values within error of the expected atmospheric composition of 295.5 [39], suggesting that excess argon is not present in these samples in detectable amounts. The generally excellent $^{40}\text{Ar}/^{39}\text{Ar}$ release characteristics and analytical parameters of these samples suggest that they are unaltered, homogeneous materials that should yield accurate ages. The best age for these samples amongst the three ages obtained for the IH experiments (integrated age, plateau age and isochron age) is taken to be the isochron age, since this computational procedure inherently accounts for deviations from ideal atmospheric composition in correcting for ‘trapped’ $^{40}\text{Ar}/^{36}\text{Ar}$ components.

Fig. 3b shows age–probability density spectra for the total-fusion analyses, with summary analytical data provided in Table 1b. A principal motivation for pursuing the single-crystal or small-population approach is to examine the grain-to-grain reproducibility of the samples. Homogeneity is verified by the generally near-Gaussian shape of the age–probability density spectra, in which only a single well-defined mode is present. Weighted mean ages of the TF experiments agree with IH ages within analytical error. Uncertainties in the weighted-mean TF ages are typically much greater than the corresponding uncertainties for the IH experiments, reflecting the inherent advantages of expelling adsorbed atmospheric argon in the early phases of an IH experiment (thus requiring a smaller correction for atmospheric argon), and increased measurement precision derived from greater gas yields during incremental heating of multi-grain samples. Ages derived from inverse isochron analyses of the TF data are generally in agreement with the conventionally calculated TF ages. As with the IH results, the best ages for the TF samples are taken to be those derived from the isochron analysis. Table 1c is a compilation of the ages used in the interpretation of the Ol Njorowa Gorge record.

4.2. Reconstruction of lake-level fluctuations

The oldest units exposed in the Ol Njorowa Gorge are silicic lava flows and intercalated pyroclastics, several tens of meters thick. The lateral

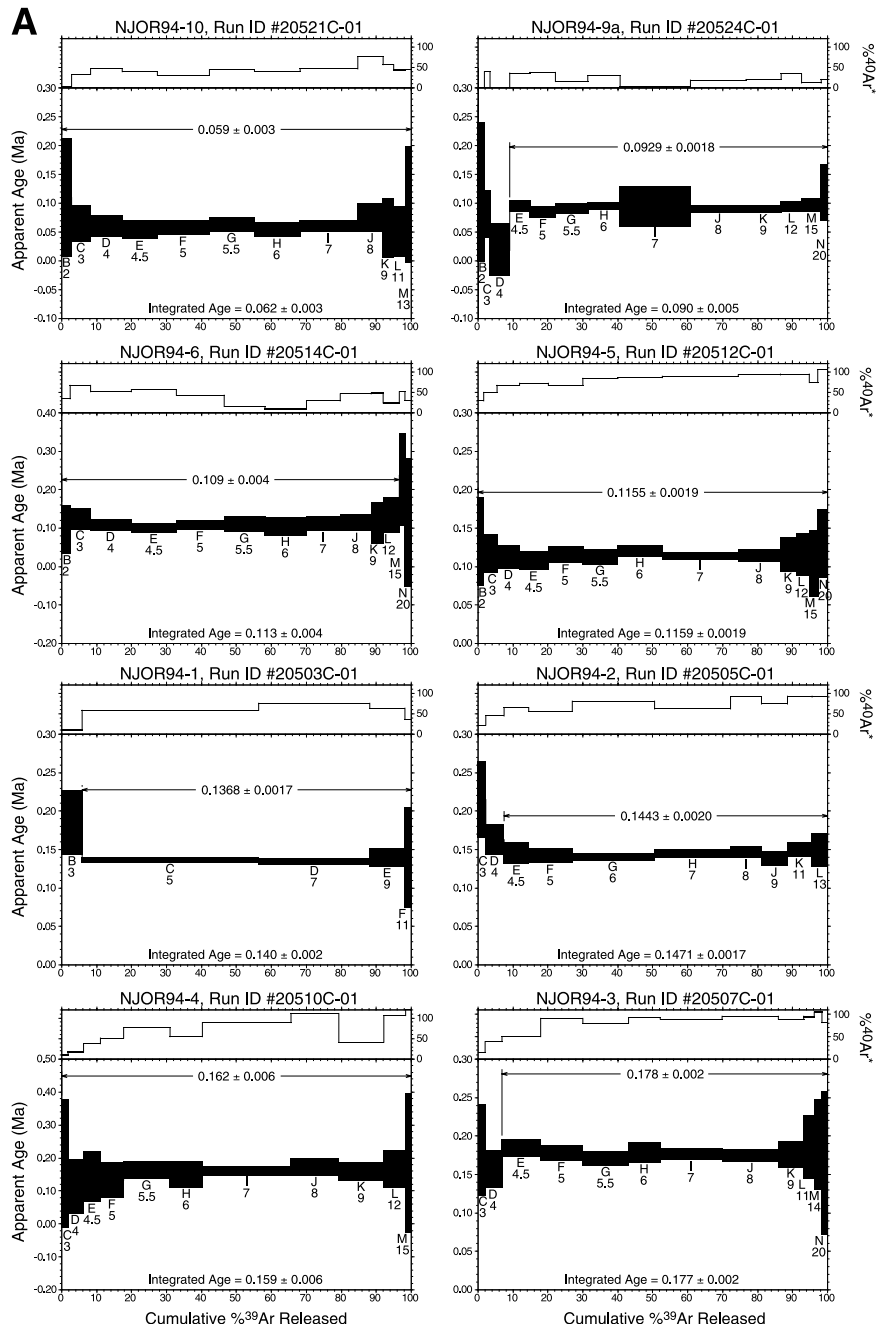


Fig. 3. (a) Results of IH analyses for the Ol Njorowa Gorge tephra. (b) Age–probability spectra for the Ol Njorowa Gorge tephra. The vertical axis of the plot is a relative probability measure of obtaining a particular age for given sample, based on the sum of the Gaussian errors of the individual single-crystal analyses. The location of the weighted mean and 1σ standard error of the weighted mean are also shown for each sample, and for the overall distribution.

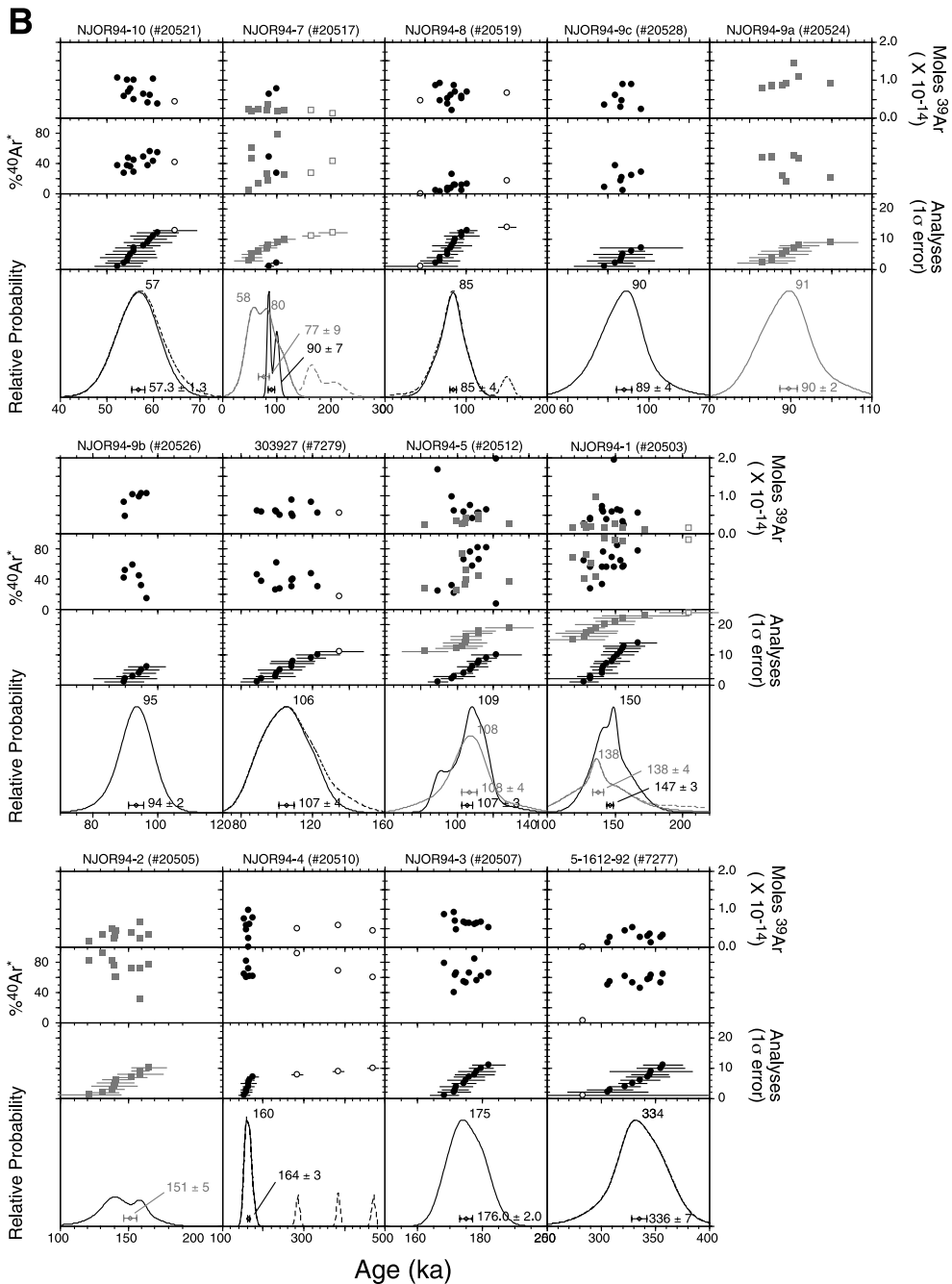


Fig. 3 (Continued).

extent of these lava flows is 6.5 km N–S and possibly greater E–W. The youngest lava flow, dated at 322 ± 20 kyr BP (Table 1c, sample 5-1612-92), is heavily eroded, and is unconformably overlain

by the oldest deposits of the Naivasha Basin. This lowest part (-58.0 to -47.0 m below the recent water level of Lake Naivasha) of the 60 m thick basin deposits consists of well-stratified airfall

Table 1a
Summary $^{40}\text{Ar}/^{39}\text{Ar}$ incremental-heating (IH)

Sample	Lab ID#	IH results			'Inverse' isochron analysis ^a		
		Integrated age ^b (ka \pm 1 σ)	Plateau age ^c (ka \pm 1 σ)	^{39}Ar in plateau (%)	MSWD ^d	$(^{40}\text{Ar}/^{36}\text{Ar})_{\text{tr}}^{\text{e}}$	Age (ka \pm 1 σ)
NJOR94-10	20521C	62 \pm 3	59 \pm 3	100	0.5	299 \pm 4	58 \pm 3
2408916 ^f	21688	81 \pm 3	80 \pm 4	66	1.0	295.8 \pm 1.0	81.7 \pm 0.8
NJOR94-7	20517C	101 \pm 30	–	–	–	–	–
NJOR94-8	20519C	66 \pm 12	73 \pm 8	65	1.5	294 \pm 2	79 \pm 9
NJOR94-9a	20524C	90 \pm 5	93 \pm 2	92	0.9	296 \pm 2	93 \pm 2
NJOR94-6	20514C	113 \pm 4	109 \pm 4	96	0.5	296 \pm 3	109 \pm 4
NJOR94-5	20512C	116 \pm 2	116 \pm 2	100	0.5	303 \pm 18	115 \pm 2
NJOR94-1	20503C	140 \pm 2	137 \pm 2	94	0.2	307 \pm 14	134 \pm 4
NJOR94-2	20505C	147 \pm 2	144 \pm 2	92	1.1	295 \pm 12	144 \pm 3
NJOR94-4	20510C	159 \pm 6	162 \pm 6	100	0.4	286 \pm 11	164 \pm 5
NJOR94-3	20507C	177 \pm 2	178 \pm 2	93	0.3	310 \pm 11	176 \pm 2

All uncertainties in ages incorporate error in calibration of J (0.3–0.6%), the neutron flux parameter. Sanidine from the Fish Canyon Tuff of Colorado was used as the monitor mineral, with a reference age of 28.02 Ma [80].

^a 'Inverse' isochron is least-squares fit line to an isotope correlation diagram in which $^{36}\text{Ar}/^{40}\text{Ar}$ is plotted against $^{39}\text{Ar}/^{40}\text{Ar}$, after corrections for neutron-induced interfering isotopes and mass spectrometer measurement bias (discrimination) are performed.

^b Integrated age is obtained from the weighted mean $^{40}\text{Ar}^*/^{39}\text{Ar}$ ratio of all steps, in which the weighting factor is the fraction of ^{39}Ar released in a individual step relative to the total ^{39}Ar released.

^c Plateau age is obtained from the weighted mean $^{40}\text{Ar}^*/^{39}\text{Ar}$ ratio of all plateau steps, in which the weighting factor is the inverse analytical variance of an individual step. Plateaus are defined as three or more contiguous gas fractions whose ages do not differ at the 95% confidence level, and which in sum comprise at least 50% of the total ^{39}Ar released from the sample [81].

^d Mean sum of weighted deviates.

^e $(^{40}\text{Ar}/^{36}\text{Ar})_{\text{tr}}$ is 'trapped' $^{40}\text{Ar}/^{36}\text{Ar}$.

^f The bulk IH result is substantially older than the total-fusion, single-crystal result, possibly resulting from the presence of anomalously old grains (xenocrysts or grains bearing excess Ar) similar to those noted during the single-crystal experiments. This IH result is not incorporated into the table of combined results (Table 1c).

tuffs and pyroclastic flow deposits containing fresh dark-gray lapilli. A coarse-grained lapilli tuff in this lowermost sequence (–54.5 m) yielded an age of 176 \pm 2 kyr BP (sample NJOR94-3), documenting prevailing subaerial conditions during the earliest basin history. The youngest pyroclastics (–47.0 m) of this early subaerial sequence were dated at 161 \pm 4 kyr BP (sample NJOR94-4). Marked erosion followed deposition of this unit.

The first manifestation of lacustrine conditions is provided by a 1.2 m thick bed of reworked pyroclastic material (–47.0 to –45.8 m) that unconformably overlies the airfall tuffs. These buff-colored deposits mainly consist of obsidian clasts and rare lapilli in a fine-grained matrix of ash and diatomaceous clay. The ages of the lapilli are between 151 \pm 5 and 144 \pm 6 kyr BP (Table 1a,b, sample NJOR94-2) with a best estimate of 146 \pm 2 kyr BP (Table 1c). The 146 \pm 2 kyr old

diatomaceous clays grade upwards into a 3.3 m thick diatomite bed (–45.8 to –42.3 m). The diatom assemblages within these clays are dominated by *Epithemia adnata*, *E. sorex* and *Fragilaria construens* and indicate a shallow freshwater lake with an approximately neutral pH [38,40]. In addition, planktonic species such as *Nitzschia lancetula* and *Aulacosira granulata* occur as minor constituents. The diatom flora and facies patterns indicate a marginal environment which is a large lake that deepened northwards (highstand V). A tuff (–44.9 m) within this pure white diatomite yields an age of 141 \pm 3 kyr BP as the best estimate (sample NJOR94-1). Interestingly, all diatomites in the section are cemented by halite; no carbonate was observed in these sediments. The diatom assemblages between –45.8 and –42.3 m are dominated by planktonic species such as *Aulacoseira granulata* and *A. goetzeana*, suggesting a

Table 1b
Summary $^{40}\text{Ar}/^{39}\text{Ar}$ total-fusion (TF) results

Sample	Lab ID#	TF results				'Inverse' isochron analysis ^a		
		Ca/K	n/n_0	Wtd. mean age (ka \pm 1 σ) ^d	MSWD	MSWD ^b	($^{40}\text{Ar}/^{36}\text{Ar}$) _{tr} ^c	Age (ka \pm 1 σ)
NJOR94-10	20521	0.070	12/13	57.3 \pm 1.3	0.7	0.4	282 \pm 9	61 \pm 3
2208916	21686	0.043	16/17	65 \pm 3	1.5	2.0	300 \pm 3	59 \pm 4
24089110	21676	0.024	40/41	75.1 \pm 1.7	1.6	2.4	298.2 \pm 1.4	72.7 \pm 1.8
2408916	21690	0.025	18/19	81 \pm 3	1.5	1.1	299.7 \pm 1.0	72 \pm 3
NJOR94-7-	20517	–	8/10	(77 \pm 9)	1.8	3.8	295 \pm 9	(77 \pm 11)
NJOR94-7	20517	0.037	2/2	(90 \pm 7)	–	–	–	–
22089115	21673/4	0.043	18/19	82 \pm 3	1.5	2.5	297 \pm 2	81 \pm 4
NJOR94-8	20519	0.130	12/14	85 \pm 4	1.1	0.8	291.8 \pm 1.6	98 \pm 6
NJOR94-9c	20528	0.038	7/7	89 \pm 4	0.5	0.3	295 \pm 2	89 \pm 4
NJOR94-9a	20524	0.013	8/8	90 \pm 2	1.0	1.0	299 \pm 4	88 \pm 3
NJOR94-9b	20526	0.069	6/7	94 \pm 2	0.5	0.2	298 \pm 3	93 \pm 3
303927-	7279	0.050	10/11	107 \pm 4	1.4	1.8	312 \pm 15	97 \pm 9
2502923	21687/91	0.058	21/22	116 \pm 4	1.5	2.2	299 \pm 3	108 \pm 7
NJOR94-5-	20512	–	9/9	108 \pm 4	1.2	1.6	295 \pm 15	108 \pm 8
NJOR94-5	20512	0.030	10/10	107 \pm 3	2.3	5.5	292 \pm 4	108 \pm 3
NJOR94-1-	20503	0.000	9/10	138 \pm 4	0.8	0.6	280 \pm 14	146 \pm 8
NJOR94-1	20503	0.000	14/14	147 \pm 3	1.2	1.4	285 \pm 7	152 \pm 4
NJOR94-1-	21388	0.002	17/20	137 \pm 4	0.9	0.8	284 \pm 10	142 \pm 5
NJOR94-2-	20505	0.001	10/11	151 \pm 5	1.5	2.0	324 \pm 22	144 \pm 6
NJOR94-2-	21384	0.004	20/21	150 \pm 2	1.3	1.6	304 \pm 7	148 \pm 3
NJOR94-4	20510	0.007	7/10	164 \pm 3	1.4	1.8	327 \pm 26	155 \pm 8
NJOR94-3	20507	0.002	11/11	176 \pm 2	1.2	1.6	298 \pm 8	175 \pm 4
5-1612-92-	7277	0.010	10/10	336 \pm 7	1.0	1.1	309 \pm 26	322 \pm 20

^c indicates results from single crystals; all other TF results are from analyses of small populations of grains (three to eight crystals). Ca/K is obtained from $^{37}\text{Ar}/^{39}\text{Ar}$ using a calibrated multiplication factor of 1.97; where indicated by '–', the value could not be determined due to excessive decay of ^{37}Ar . ' n/n_0 ' indicates number of analyses accepted as reflecting only primary juvenile feldspars (and used in the subsequent statistical analyses), over the total number of analyses performed. The weighted mean TF age is calculated using the inverse variance of the individual analyses as the weighting factor; the uncertainty is the 1 σ standard error of the mean, derived from the maximum of either the conventional weighted standard error of the mean formula [82], or a formula that incorporates excess scatter beyond that predicted by the analytical uncertainties alone [83]. See Table 1a for additional notes.

^a 'Inverse' isochron is least-squares fit line to an isotope correlation diagram in which $^{36}\text{Ar}/^{40}\text{Ar}$ is plotted against $^{39}\text{Ar}/^{40}\text{Ar}$, after corrections for neutron-induced interfering isotopes and mass spectrometer measurement bias (discrimination) are performed.

^b Mean sum of weighted deviates.

^c ($^{40}\text{Ar}/^{36}\text{Ar}$)_{tr} is 'trapped' $^{40}\text{Ar}/^{36}\text{Ar}$.

^d Integrated age is obtained from the weighted mean $^{40}\text{Ar}^*/^{39}\text{Ar}$ ratio of all steps, in which the weighting factor is the fraction of ^{39}Ar released in an individual step relative to the total ^{39}Ar released.

large lake with circumneutral pH. At approximately –43.6 m, fossil diatoms document the lowest pH (7.2) and highest lake level of the entire record.

Assuming that the average sedimentation rate for diatomites is 1 mm yr^{–1}, the timespan between the deposition of the 141 \pm 3 kyr BP tuff and the 1.3 m higher diatomite sample is in the order of 1300 yr, i.e. at about 139 kyr BP. Although sed-

imentation rates for diatomite are usually lower in most lakes (much less than 1 mm yr^{–1}, [41]), rates in East African rift lakes may be as high as 10 mm yr^{–1} due to enriched silica supply from hot springs [42]. Taking into account the uncertainties in $^{40}\text{Ar}/^{39}\text{Ar}$ dating and determination of sedimentation rates, the best estimate for the peak highstand is between 139 and 133 kyr BP.

Termination of the lake-level highstand at

Table 1c
Combined laser-fusion and integrated-heating $^{40}\text{Ar}/^{39}\text{Ar}$ ages

Sample	Strat. interval (m)	Age (ka \pm 1 σ)
NJOR94-10	+2.4	60 \pm 2
2208916*		59 \pm 4
24089110*		72.7 \pm 1.8
2408916 (tf)*		73 \pm 3
22089115*		81 \pm 4
NJOR94-8	–16.6	92 \pm 5
NJOR94-9c*	–19.0	89 \pm 4
NJOR94-9a	–19.5	91 \pm 2
NJOR94-9b*	–19.7	93 \pm 3
303927/NJOR94-6	–22.9 to –32.9	107 \pm 4
2502923*		108 \pm 7
NJOR94-5	–38.8	113 \pm 2
NJOR94-1	–43.6	141 \pm 3
NJOR94-2	–44.9	146 \pm 2
NJOR94-4	–45.8	161 \pm 4
NJOR94-3	–53.3	176 \pm 2
5-1612-92*	< –60	322 \pm 20

Stratigraphical interval is referenced to present lake level at 1890 m asl. Ages are a weighted mean combination of the IH and TF isochron results. Errors are derived from the conventional weighted standard error of the mean formula [83]. Sample NJOR94-7 yielded equivocal results for both the TF and IH experiments, and is not included here. (*) denotes total-fusion results only.

about 141 \pm 3 kyr is indicated in the upper part of the diatomite bed by fluvial deposits, rare sponge spicules, phytoliths (Cyperaceae) and diatom fragments, topped by a 113 \pm 2 kyr BP old tuff (NJOR94-5). The interpretation of a major drop in lake level is further substantiated by the presence of authigenic clinoptilolite and analcime. The disappearance of authigenic analcime and the appearance of chabazite toward the top of the unit, however, suggest a trend toward less alkaline conditions in a very shallow water body by the end of this lowstand. This is superseded by highstand IV, indicated by the deposition of the previously mentioned laminated diatomite bed, 1.6 m thick, with tuff layers containing fresh glass (–39.3 to –37.8 m). Diatom assemblages, dominated by *Gomphonema angustatum* and *G. gracile*, indicate a large shallow freshwater lake with an approximately neutral pH [40]. The diatomite bed is overlain by several beds of partly reworked, unaltered pyroclastic material (–37.8 to –33.8 m), reflecting sustained freshwater conditions during deposition.

The lowermost member (–37.8 to –36.4 m) of this pyroclastic unit was dated at 108 \pm 7 kyr BP (sample 2502923). However, in the upper part of this unit (–36.4 to –33.8 m) perlitic cracks in glass shards, abundant phytoliths and erosional unconformities herald a major regression.

Subaerial or extreme shallow-water conditions appear to have been attained at least along the periphery of the basin, immediately before a 10 m thick, 107 \pm 4 kyr BP old welded tuff (Kedong Valley Tuff) was deposited (–33.8 to –23.8 m) (samples NJOR94-6 and 0303927). This unit is overlain by a 2.5 m package of laminated siltstones (–23.5 to –21.0 m) containing chabazite and clinoptilolite, indicating prevailing alkaline conditions. These horizons are overlain by partly reworked pyroclastic deposits with unaltered volcanic glass (–21.0 to –20.5 m). In comparison with severely altered glass in other layers, the pristine condition of the glass indicates deposition in a freshwater lake, inferred to correspond to lake-level highstand III. Glass shards with perlitic cracks and montmorillonite rims indicate deposition in a freshwater lake with a pH between 8 and 9, i.e. conditions slightly more alkaline than those of the older highstands IV and V. The absence of diatomite beds during this highstand may be a function of pronounced volcanic eruptions and high sedimentation rates. The age of this highstand is constrained by three intercalated, relatively unaltered tuffs (–20.6 to –20.5 m, –20.5 to –20.0 m and –20.0 to –19.9 m, respectively) dated at 93 \pm 3, 91 \pm 2 and 89 \pm 4 kyr BP (samples NJOR94-9a, b and c). Deposits associated with a superseding lake-level lowstand contain chabazite, clinoptilolite and analcime (–19.9 to –13.4 m). Finely laminated siltstones and siltstones with mud cracks and impact marks of airfall lapilli suggest alternating subaerial and shallow water conditions. A thin tuff layer (–17.2 m) was dated at 92 \pm 5 kyr BP, providing an age for the most extreme lowstand (sample NJOR94-8).

Toward the top, three diatomite beds, up to 16 cm thick and intercalated by 81 \pm 4 kyr BP old tephra (–13.1 m, sample 22089115), document highstand II. The diatom assemblages are characterized by *Fragilaria construens*, *F. brevistriata* and *F. pinnata*, which reflect shallow freshwater

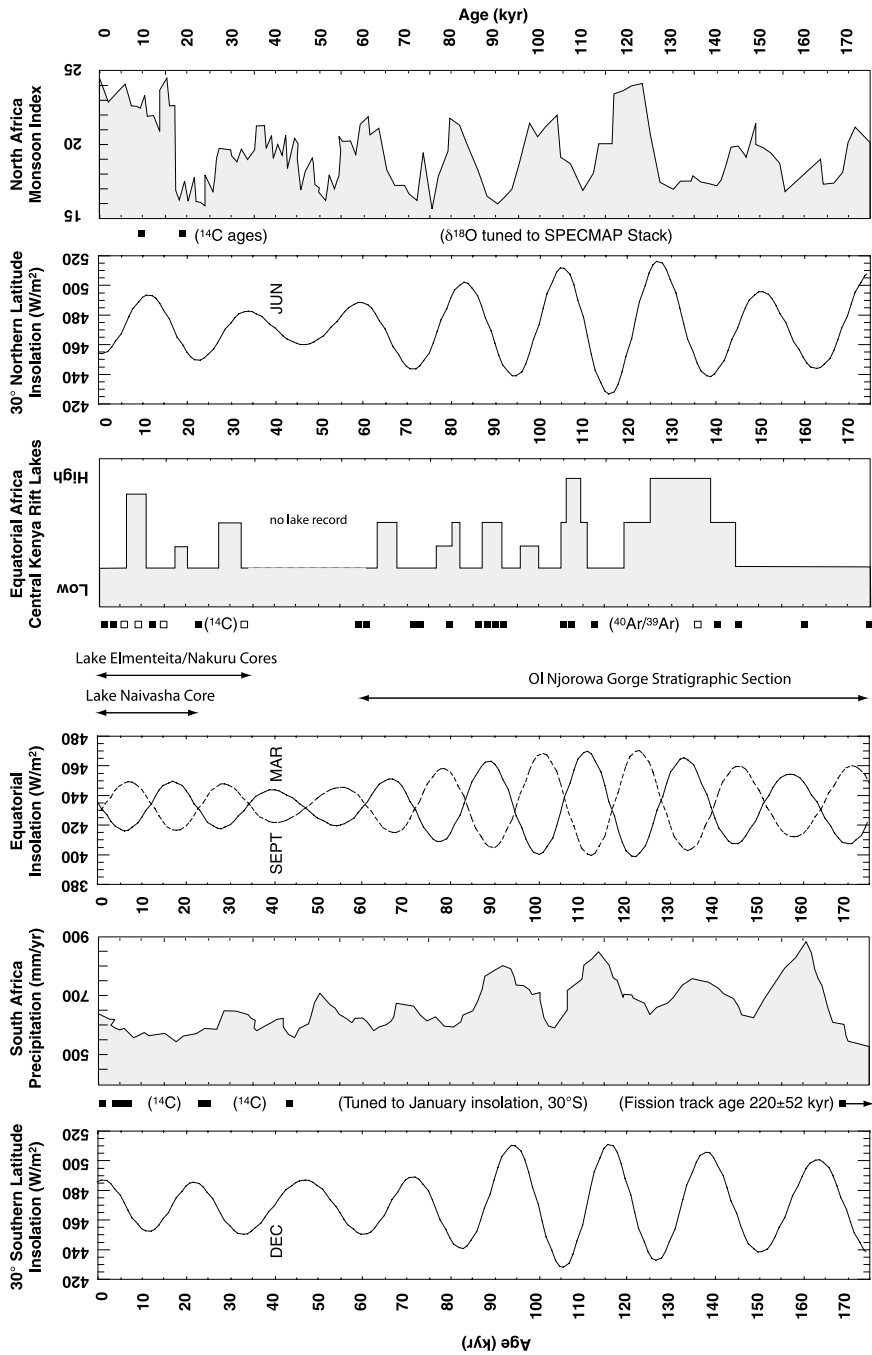


Fig. 4. Correlation of East African high lake levels and insolation changes. (1) South African paleo-precipitation record from the Pretoria Saltpan [6], (2) East African Central Kenya Rift lake-level records including data from Lake Naivasha, Lake Nakuru and Lake Elmenteita ([8,19,45] and this work), (3) North Africa Monsoon Index from deep-sea sediment core RC24-07 [5]. Insolation data from [4]. Squares indicate age control points from ^{14}C , fission track and $^{40}\text{Ar}/^{39}\text{Ar}$ dating; for the Central Kenya Rift lakes, empty squares indicate age data from the Nakuru–Elmenteita Basin, filled squares represent ages from the Naivasha Basin.

conditions along the southern basin margin. The presence of *Aulacosira granulata* and related species suggests a connection to deeper lake water farther north. However, in contrast to the older diatomites the occurrence of *Thalassiosira faurii*, *Mastogloia smithi*, *M. elliptica* and *Anomoeoneis sphaerophora* documents slightly alkaline conditions with a pH just above 8. Diatomite deposition was terminated by increasing volcanic activity, as recorded by several tuff layers in the –12.8 to –6.9 m interval. Clinoptilolite and analcime in the lower part of this pyroclastic section document rapidly increasing alkalinity in the course of lake regression. Numerous fluorite concretions attest to an increasing influence of hot-spring activity along the lake shores. Intermittent, less alkaline phases are represented by the substitution of analcime by chabazite within partly reworked tuff layers. However, severe alteration and formation of analcime above these layers shows a return to strongly alkaline conditions and a pronounced lake-level lowstand. Dated horizons at 73 ± 3 and 72.7 ± 1.8 kyr (samples 2408916 and 24089110) constrain the timing of this interval of shallow lake conditions and higher alkalinity (–11.4 to –9.6 and –8.2 to –7.2 m, respectively).

The upper part of the 5.5 m thick pyroclastic sequence as well as overlying reworked tuffs (–6.9 to –5.2 m) contain unaltered glass shards, representing a renewed freshening of the lake (pH < 9). This is interpreted to correspond to lake-level highstand I. Above this unit follow subaerially deposited gray airfall tuffs, 4.5 m thick and 59 ± 4 kyr BP old (–5.2 to –1.1 m, sample 2208916), with an intense yellowish hue in the uppermost horizons. These zones contain analcime, similar to an overlying waterlaid tuff. The overlying pyroclastic and siltstone beds (–1.2 to +2.4 m above the recent lake level) contain variable amounts of authigenic silicates. Yellow tuffs in excess of 10 m thickness in the upper part of this sequence (>2.4 m) attest to a pronounced period of high alkalinity during a major drop in lake level at 60 ± 2 kyr BP (sample NJOR94-10). These yellow pyroclastics are strongly eroded along the top. By about 60 kyr the ultimate Pleistocene regression of the lake shore was complete [8]. Intense volcanic activity created the comen-

ditic flows and eruptive centers of the Olkaria Volcanic Complex, which were partly inundated by the lake-level highstand at 10–6 kyr BP, forming well-preserved shorelines and sediments [24].

5. Discussion and conclusions

Structural relationships in the Naivasha Basin show that this region was not affected by pronounced tectonic movements or volcanic activity after the closure of the basin at 322 ± 20 kyr BP and before the rhyolitic Olkaria Volcanic Complex had formed at ~ 20 kyr BP [8,23,43,44]. Eruptive activity of the adjacent Mt. Longonot trachytic volcano during this timespan produced most of the waterlaid tephra exposed in the Ol Njorowa Gorge [19,23]. However, since Mt. Longonot is located in the southeastern corner of the Naivasha Basin and the major part of the catchment lies to the northeast of the present lake, we infer that this volcanic activity did not generate important changes in drainage patterns and lake levels (Fig. 1c). The lake-level fluctuations recorded in the 60 m thick Ol Njorowa Gorge sediments therefore reflect important changes in the precipitation and evaporation balance. Together with lake-level records derived from several sediment cores from the Naivasha and Elementeita–Nakuru basins [45], this chronology provides a paleoclimate record for equatorial East Africa for the last two glacial–interglacial cycles, i.e. MIS 6–1 (Fig. 4). Interestingly, after the formation of the Naivasha Basin, there is no evidence for a larger lake during the interglacials corresponding to MIS 9 (~ 336 – 305 kyr BP; [46]) and MIS 7 (~ 237 – 228 kyr BP; [47]). The first highstand of Lake Naivasha occurs at the MIS 6–5 transition and persists for 25 kyr (between 146 and 120 kyr BP, with a maximum at around 139–133 kyr BP), which correlates with highstands in other rift-valley lakes (Fig. 1). Uranium-series ages for hydrothermal deposits recording geothermal activity in the Suguta Valley (Northern Kenya Rift) suggest elevated water tables and increased availability of meteoric water associated with more humid climate as early as 133 ± 11 kyr BP [13]. High lake levels can be in-

ferred from shorelines in the Magadi–Natron Basin in the southern part of the rift, where littoral stromatolites provide U-series ages of 135 ± 10 kyr BP [12]. There is also corroborative evidence for lake highstands in Lake Turkana around 130 kyr BP [11]. The younger periods of increased humidity at around 113–108, ~ 91 and ~ 66 kyr BP as recorded in the Naivasha sediments have not been reported from other East African lake basins.

There is no clear evidence for high lakes in the Central Kenya Rift (i.e. Lakes Naivasha, Nakuru and Elmenteita) between 60 and 30 kyr BP. The oldest highstand after 30 kyr BP is documented in the Nakuru–Elmenteita Basin between 30 and 28.5 kyr BP [45] (Fig. 4). During this time, slightly higher lake levels were reported for Lake Manyara some 400 km south of Lake Naivasha, as indicated by diatom assemblages, clay minerals and stromatolites 20 m above the present lake [48–51]. Similar histories are known for Lake Albert [50,52,53] and paleo-lake Suguta south of Lake Turkana [54]. The Naivasha record by Richardson and Dussinger [45] begins at around 24.5 kyr BP, from which a higher water level at 21–17.5 kyr BP can be inferred. This highstand correlates with a higher precipitation/evaporation ratio in the Tanganyika Basin at about the same time [55]. The most recent highstand in the Central Kenya Rift occurs between 10 and 6 kyr BP [24,45,56], which correlates with a humid period as documented in other East African lake basins [55] and ice cores from Mt. Kilimanjaro [57]. During this highstand, Lake Naivasha and Lake Nakuru–Elmenteita were more than 100 m deep, the areal extent of the lakes was larger by a factor 3–4, and the volume of the water bodies 50–60 times greater [25]. Lake-balance modeling suggests a 16–32% increase in precipitation during the Early Holocene [25,58,59].

The chronology of highstands at 10–11 kyr intervals suggests a strengthening of both spring and fall rains, which were triggered by increased March or September insolation on the equator at every half-precession cycle (Fig. 4). This suggests that orbitally induced changes in solar radiation certainly account for a large part of hydrological changes in East Africa. Such radiation changes

could cause a relatively large increase in spring temperatures over land and therefore an intensification of the intertropical convergence and convective rainfall in this region. Water-balance modeling of the ~ 135 kyr old paleo-Lake Naivasha suggests a minimum 11% increase in precipitation compared to the modern values [25]. Including a vegetation feedback into the model, the basin could have received even 28% more rainfall. These simulations also suggest that evaporation is an important factor in the hydrological budget. In the modern lake area, potential evapotranspiration is three times higher than precipitation [27]. The extremely low solar radiation during the dry season between 139 and 133 kyr BP causing reduced evaporation may also have contributed to the positive hydrological budget of paleo-Lake Naivasha [4,25]. Whereas the climate dynamics during the penultimate deglaciation and the last interglacial between 146 and 60 kyr BP seem to be similar to the modern conditions, the causal links between East African climate and insolation after 60 kyr BP were different from today (Fig. 4). The minor highstand at around 21–17.5 kyr BP seems to be consistent with a strong ITCZ caused by maximum March insolation on the equator. In contrast, highstands at 30–28.5 kyr BP and 10–6 kyr BP suggest a more complex link between insolation and climate change in East Africa. These well-dated periods of increased humidity are out of phase with maximum March insolation and significantly lead maximum December insolation on the equator. A potential mechanism to explain this phenomenon could involve an enhanced moisture transport caused by maximum Northern Hemisphere June–July insolation and a stronger boreal summer monsoonal circulation.

Compared to other records of African climate change, the most relevant other continental record comes from Lake Abhé in northern Ethiopia and only extends back to ~ 70 kyr BP, with good age control to ~ 40 kyr BP [9]. The timing of humid and dry periods appears to be consistent with a strong summer monsoon controlled by Northern Hemisphere summer insolation. Such a link between insolation and North African climate has also been proposed by Molino and McIntyre [5] based on fossil faunal assemblage variations in

deep-sea sediment core RC24-07 (Fig. 4). This record contains two ^{14}C ages of 18.7 and 9.4 kyr BP at 73 and 33 cm core depth, whereas the older part of the chronology was tuned to the SPECMAP chronology [60]. The Pretoria Saltpan time series of summer precipitation in South Africa [6] covers approximately the last 200 kyr, but only provides radiocarbon ages to about 43 kyr BP (Fig. 4). The lower part of the record was tuned using a fission-track age for the formation of the Saltpan Basin of around 220 ± 52 kyr BP. A new record for environmental change in the southern tropics over the last 150 kyr derives from Lake Tritrivakely, Madagascar, but is tuned to the Vostok δD isotopic temperature records beyond 41 kyr BP [10]. These records correlate with the chronology of arid episodes recorded in eolian sediments from the Mega Kalahari sand sea [61], suggesting strong coupling between climate and Southern Hemisphere summer insolation, out of phase with North African paleo-monsoon indices [1,5,62] (Fig. 4).

The Naivasha lake-level record also has important implications for the current discussion of a tropical or Southern Hemisphere forcing of deglaciation. The key argument of this hypothesis is that tropical SSTs lead high-latitude Northern Hemisphere ice volume by several thousand years [16,17]. Traditional Milankovitch theory [63] suggests that summer insolation at mid-latitudes ($60\text{--}65^\circ\text{N}$) in the Northern Hemisphere directly triggers ice-age climate cycles. Based on this hypothesis, the widely quoted SPECMAP timescale [60] for Pleistocene ice-volume variations (as recorded by marine $\delta^{18}\text{O}$) uses a value of 127 kyr BP as the midpoint of the penultimate deglaciation (i.e. Termination II, [64]). However, new U–Th age determinations from corals and associated sediments in western Australia [65,66], Papua New Guinea [67,68], Indonesia [69] and the Bahamas [14] suggest a more complex linkage between insolation and the ice-age cycles, most likely including processes sourced in the tropics or the Southern Hemisphere [14,16]. The coral-reef terraces and glacio-eustatic sea-level change recorded therein provided U–Th ages greater than 130 kyr in several regions [14,66–68]; however, the best estimate for Termination II as determined by Henderson

and Slowey [14] is 135 ± 2.5 kyr BP. This age seems to be consistent with early Vostok chronologies placing the age for Termination II in the $\delta^{18}\text{O}$ record at ~ 133 kyr [70,71], i.e. after a 2 kyr lag due to the atmospheric residence time of O_2 [64]. Atmospheric warming again leads global ice volume by $\sim 3\text{--}4$ kyr as recorded in the Vostok δD record, suggesting the midpoint at 139–138 kyr [70]. In contrast, the 142 kyr BP midpoint of the well-dated Devils Hole record [72,73] is still significantly older than the marine $\delta^{18}\text{O}$ chronologies.

The Naivasha record at Termination II is fully consistent with these new chronologies and interpretations. The most dramatic change in the paleo-hydrology occurs as early as at 146 ± 2 kyr BP at the beginning of the lake-level highstand between 139 and 133 kyr BP. Synchronous major shifts toward increased humidity have also been determined in northern and southern Africa, where several lacustrine records and coastal marine cores suggest positive hydroclimatic conditions at around 135 kyr BP [6,10,74–76]. These African records strongly support the concept of a direct relationship between increased insolation heating and convective rainfall over low-latitude land masses and a less direct connection with melting of Northern Hemisphere ice sheets. Several hypotheses have been proposed to explain how variations in Earth's precession and environmental changes in the tropics can account for the termination of glaciations [77–79]. One potential mechanism attributes the changes in higher latitudes to precessional forcing of the interaction between an altered seasonal cycle and the ENSO [77]. A strong ENSO at the end of the penultimate glacial could reduce the Hadley circulation and therefore the intensity of poleward transports of heat and moisture, which in turn could help explain the decay of ice sheets in North America [77]. An alternative mechanism for tropical forcing of deglaciation involves variations in methane (CH_4) sources in Africa and South America [78,79]. It has been shown, for example, that CH_4 fluctuations recorded in Greenland ice cores coincide with episodes of drought in tropical Africa and Tibet at the time of Termination I [78,79]. Taking into account the early change in African

climate at Termination II, the latter hypothesis could also provide a potential mechanism for a tropical forcing of deglaciation at around 135 kyr BP.

Acknowledgements

This project was funded by two grants to M.T. and M.S. by the German Research Foundation (DFG). We thank the government of Kenya and the Kenya Wildlife Service for research permits and support. The authors gratefully acknowledge F. Gasse and F. Chalié for help with diatom taxonomy and interpretation as well as for many inspiring discussions. We also acknowledge the editor E. Bard, the two reviewers F. Gasse and P. Barker as well as the anonymous reviewer for their helpful comments on the manuscript. We also thank P. Barker, R. Becht, S. Gaciri, G. Henderson, D. Livingstone, S. Lorenz, G. Muchemi, R. Schneider, R. Telford and D. Verschuren for discussions. We also thank S. Higgins, S. Kabinigu, T. Schlüter and M. Ibs-von Seht for logistical support. **[BARD]**

References

- [1] M. Rossignol-Strick, African monsoons, an immediate climate response to orbital insolation, *Nature* 304 (1983) 46–49.
- [2] J.E. Kutzbach, F.A. Street-Perrott, Milankovitch forcing of fluctuations in the level of tropical lakes from 18 to 0 kyr BP, *Nature* 317 (1985) 130–134.
- [3] S. Clemens, W. Prell, D. Murray, G. Shimmield, G. Weedon, Forcing mechanisms of the Indian Ocean monsoon, *Nature* 353 (1991) 720–725.
- [4] A. Berger, Long-term variations of daily insolation and Quaternary climatic changes, *J. Atmos. Sci.* 35 (1978) 2362–2367.
- [5] B. Molino, A. McIntyre, Nutricline variation in the equatorial Atlantic coincident with the Younger Dryas, *Paleoceanography* 5 (1990) 997–1008.
- [6] T.C. Partridge, P.B. deMenocal, S.A. Lorentz, M.J. Paiker, J.C. Vogel, Orbital forcing of climate over South Africa: a 200,000-year rainfall record from the Pretoria Saltpan, *Quat. Sci. Rev.* 16 (1997) 1125–1133.
- [7] F. Gasse, Hydrological changes in the African tropics since the Last Glacial Maximum, *Quat. Sci. Rev.* 19 (2000) 189–211.
- [8] M.H. Trauth, M.R. Strecker, Late Pleistocene lake-level fluctuations in the Naivasha Basin, Kenya, in: T.C. Johnson, E.O. Odada (Eds.), *The Limnology, Climatology and Paleoclimatology of the East African Lakes*, The International Decade for the East African Lakes (IDEAL), Gordon and Breach, Newark, NJ, 1996, pp. 549–557.
- [9] F. Gasse, Evolution of Lake Abhé (Ethiopia and TFAI), from 70,000 b.p., *Nature* 265 (1977) 42–45.
- [10] F. Gasse, E. Van Campo, Late Quaternary environmental changes from a pollen and diatom record in the southern tropics (Lake Tritrivakely, Madagascar), *Palaeogeogr. Palaeoclimatol. Palaeoecol.* 167 (2001) 287–308.
- [11] K.W. Butzer, F.W. Brown, D.L. Thruher, Horizontal sediments of the lower Omo valley; the Kibish formation, *Quaternaria* 11 (1969) 15–29.
- [12] C. Hillaire-Marcel, O. Carro, J. Casanova, ^{14}C and Th/U dating of Pleistocene and Holocene stromatolites from east African paleolakes, *Quat. Res.* 25 (1986) 312–329.
- [13] N.C. Sturchio, P.N. Dunkley, M. Smith, Climate-driven variations in geothermal activity in the northern Kenya rift valley, *Nature* 362 (1993) 233–234.
- [14] G.M. Henderson, N.C. Slowey, Evidence from U-Th dating against Northern Hemisphere forcing of the penultimate deglaciation, *Nature* 404 (2000) 61–66.
- [15] R.B. Alley, E.J. Brook, S. Anandakrishnan, A northern lead in the orbital band north-south phasing of Ice-Age events, *Quat. Sci. Rev.* 21 (2002) 431–441.
- [16] D.W. Lea, D.K. Pak, H.J. Spero, Climate impact of Late Quaternary equatorial Pacific sea surface temperature variations, *Science* 289 (2000) 1719–1724.
- [17] T.D. Herbert, J.D. Schuffert, D. Andreasen, L. Heusser, M. Lyle, A. Mix, A.C. Ravelo, L.D. Stott, J.C. Herguera, Collapse of the California current during glacial maxima linked to climate change on land, *Science* 293 (2001) 71–76.
- [18] D.P. Schrag, Of ice and elephants, *Nature* 404 (2000) 23–24.
- [19] M.H. Trauth, A. Deino, M.R. Strecker, Response of the East African climate to orbital forcing during the Last Interglacial (130–117 kyr BP) and the early Last Glacial (117–60 kyr BP), *Geology* 29 (2001) 499–502.
- [20] G.R. McGregor, S. Nieuwolt, *Tropical Climatology: An Introduction to the Climates of the Low Latitudes*, Wiley, Chichester, 1998, 352 pp.
- [21] S.E. Nicholson, A review of climate dynamics and climate variability in Eastern Africa, in: T.C. Johnson, E.O. Odada (Eds.), *The Limnology, Climatology and Paleoclimatology of the East African Lakes*, The International Decade for the East African Lakes (IDEAL), Gordon and Breach, Newark, NJ, 1996, pp. 25–56.
- [22] S.C. Scott, The geology of Mt. Longonot Volcano, central Kenya; a question of volumes, *Philos. Trans. R. Soc. London* 296 (1980) 437–465.
- [23] M.C.G. Clarke, D.G. Woodhall, D. Allen, G. Darling, Geological, volcanological and hydrogeological controls on the occurrence of geothermal activity in the area sur-

- rounding Lake Naivasha, Kenya, Ministry of Energy, Nairobi, Kenya, 1990, 138 pp.
- [24] C.K. Washbourn-Kamau, The Ol Njorowa Gorge, Lake Naivasha Basin, Kenya, in: D.C. Greer (Ed.), *Desertic Terminal Lakes*, Utah Water Research Laboratory, 1977, pp. 297–307.
- [25] A.G.N. Bergner, M.H. Trauth, B. Bookhagen, B., Modeling ~135 and 9 kyr old highstands of Lake Naivasha, Central Kenya Rift, *Glob. Planet. Change* (2002), in press.
- [26] L.E. Åse, A note on the water budget of Lake Naivasha, *Geogr. Ann.* 69A (1987) 415–429.
- [27] Kenya Meteorological Department, Synoptic and rain station data, Ministry of Information, Transport and Communications, Nairobi, Kenya, 2000, unpublished.
- [28] S. Roessner, M. Strecker, Late Cenozoic tectonics and denudation in the Central Kenya Rift: quantification of longterm denudation rates, *Tectonophysics* 278 (1997) 83–94.
- [29] W. Sharp, A.L. Deino, CO₂ laser heating of samples for Ar-Ar geochronology, *EOS Trans. AGU* 77 (1996) F773.
- [30] P.R. Renne, C.C. Swisher, A.L. Deino, D.B. Karner, T.L. Owens, D.J. DePaolo, Intercalibration of standards, absolute ages and uncertainties in ⁴⁰Ar/³⁹Ar dating, *Chem. Geol.* 145 (1998) 117–152.
- [31] A. Deino, P. Potts, Single-crystal ⁴⁰Ar/³⁹Ar dating of the Ologesailie Formation, Southern Kenya Rift, *J. Geophys. Res.* 95 (1990) 8453–8470.
- [32] A.L. Deino, P.R. Renne, C.C. Swisher III, ⁴⁰Ar/³⁹Ar dating in paleoanthropology and archaeology, *Evol. Anthropol.* 6 (1998) 63–75.
- [33] M. Utada, Zeolites in sedimentary rocks, with reference to the depositional environments and zonal distribution, *Sedimentology* 7 (1966) 237–257.
- [34] R.C. Surdam, R.A. Sheppard, Zeolites in saline, alkaline lake deposits, in: L.B. Sand, F.A. Mumpton (Eds.), *Natural Zeolites: Occurrence, Properties, Use*, Pergamon Press, Oxford, 1978, pp. 145–175.
- [35] L.B. Sand, F.A. Mumpton (Eds.), *Natural Zeolites: Occurrence, Properties, Use*, Pergamon Press, Oxford, 1978, 546 pp.
- [36] R.W. Renaut, Zeolitic diagenesis of late Quaternary fluviolacustrine sediments and associated calcrete formation in the Lake Bogoria Basin, Kenya Rift Valley, *Sedimentology* 40 (1993) 271–301.
- [37] A. Hall, Zeolitization of volcanoclastic sediments: The role of temperature and pH, *J. Sediment. Res.* 68 (1998) 739–745.
- [38] F. Gasse, *East African Diatoms. Taxonomy, Ecological Distribution*, J. Cramer, Berlin, 1986, 201 pp.
- [39] R.H. Steiger, E. Jäger, Subcommittee on geochronology: Convention on the use of decay constants in geo- and cosmochronology, *Earth Planet. Sci. Lett.* 36 (1977) 359–362.
- [40] F. Gasse, S. Juggins, L. BenKhelifa, Diatom-based transfer functions for inferring past hydrochemical characteristics of African lakes, *Palaeogeogr. Palaeoclimatol. Palaeoecol.* 117 (1995) 31–54.
- [41] G. Einsele, *Sedimentary Basins, Evolution, Facies and Sediment Budget*, Springer, Berlin, 2000, 792 pp.
- [42] R.J. Telford, H.F. Lamb, Groundwater-mediated response to Holocene climatic change recorded by the diatom stratigraphy of an Ethiopian crater lake, *Quat. Res.* 52 (1999) 63–75.
- [43] M.R. Strecker, P.M. Blisniuk, G.H. Eisbacher, Rotation of extension direction in the central Kenya Rift, *Geology* 18 (1990) 299–302.
- [44] W. Bosworth, M. Strecker, Stress field changes in the Afro-Arabian Rift System during the Miocene and to recent period, *Tectonophysics* 278 (1997) 47–62.
- [45] J.L. Richardson, R.A. Dussinger, Paleolimnology of mid-elevation lakes in the Kenya Rift Valley, *Hydrobiologia* 143 (1986) 167–174.
- [46] N.J. Shackleton, The 100,000-year ice-age cycle identified and found to lag temperature, carbon dioxide and orbital eccentricity, *Science* 289 (2000) 1897–1902.
- [47] L.F. Robinson, G.M. Henderson, N.C. Slowey, U-Th dating of marine isotope stage 7 in Bahamas slope sediments, *Earth Planet. Sci. Lett.* 196 (2002) 175–187.
- [48] P. Stoffers, S. Holdship, Diagenesis of sediments in an alkaline lake Lake Manyara, Tanzania, IXth International Congress of Sedimentology, Nice, theme 7, 1975, pp. 211–217.
- [49] S.A. Holdship, The palaeolimnology of Lake Manyara, Tanzania: a diatom analysis of a 56 meter sediment core, Ph.D. Thesis, Duke University, 1976, unpublished.
- [50] P. Stoffers, A. Singer, Clay minerals in Lake Mobutu Sese Seko (Lake Albert) - their diagenetic changes as an indicator of the paleoclimate, *Geol. Rundsch.* 68 (1979) 1009–1024.
- [51] J. Casanova, J., *Les stromatolites continentaux: paléo-écologie, paléohydrologie, paléoclimatologie*, Ph.D. Thesis, Université Marseille-Luminy, 1986, unpublished.
- [52] T.J. Harvey, The paleolimnology of Lake Mobutu Sese Seko, Uganda-Zaire: the last 28000 years, Ph.D. Thesis, Duke University, 1976, unpublished.
- [53] K.R.M. Beuning, M.R. Talbot, K. Kelts, D.A. Livingstone, A revised 30,000 year paleoclimatic and paleohydrologic history of Lake Albert, Uganda, East Africa, *Palaeogeogr. Palaeoclimatol. Palaeoecol.* 136 (1997) 259–279.
- [54] J. Casanova, C. Hillaire-Marcel, N. Page, M. Tajeb, M. Vincens, Stratigraphie et paléohydrologie des épisodes lacustres du Quaternaire récent du rift Suguta (Kenya), *C.R. Acad. Sci. Paris* 307 Série II (1988) 1251–1258.
- [55] F. Gasse, V. Lédée, M. Massault, J.C. Fontes, Water-level fluctuations of Lake Tanganyika in phase with oceanic changes during the last glaciation and deglaciation, *Nature* 342 (1989) 57–59.
- [56] J.L. Richardson, A.E. Richardson, History of an African Rift lake and its climatic implications, *Ecol. Monogr.* 42 (1972) 499–534.
- [57] L.G. Thompson, E. Mosley-Thompson, M.E. Davis, K.A. Henderson, H.H. Brecher, V.S. Zagorodnov, T.A. Mashotta, P.N. Lin, V.N. Mikhalenko, D.R. Hardy, J.

- Beer, Kilimanjaro ice core records evidence of Holocene climate change in tropical Africa, *Science* 298 (2002) 589–593.
- [58] S. Hastenrath, J.E. Kutzbach, Paleoclimatic estimates from water and energy budgets of East African lakes, *Quat. Res.* 19 (1983) 141–153.
- [59] C.E. Vincent, T.D. Davies, P. Pringlecombe, A.K.C. Beresford, Lake levels and glaciers: Indicators of the changing rainfall in the mountains of East Africa, in: W.C. Mahaney (Ed.), *Quaternary and Environmental Research on East African Mountains*, York University, North York, ON, 1989, pp. 199–216.
- [60] J. Imbrie, J.D. Hays, D.G. Martinson, A. McIntyre, A.C. Mix, J.J. Morley, N.G. Pisias, W.L. Prell, N.J. Shackleton, The orbital theory of Pleistocene climate: Support from a revised chronology of the marine 18O record, in: A. Berger, J. Imbrie, J. Hays, G. Kukla, B. Saltzman (Eds.), *Milankovitch and Climate Part I*, Reidel, Dordrecht, 1984, pp. 269–305.
- [61] S. Stokes, D.S.G. Thomas, R. Washington, Multiple episodes of aridity in southern Africa since the last interglacial period, *Nature* 388 (1997) 154–158.
- [62] F.A. Street, A.T. Grove, Global maps of lake-level fluctuations since 30,000 yr BP, *Quat. Res.* 12 (1979) 83–118.
- [63] M. Milankovitch, *Mathematische Klimalehre und astronomische Theorie der Klimaschwankungen*, in: W. Köppen, R. Geiger (Eds.), *Handbuch der Klimatologie*, Gebürder Borntraeger, 1930, 176 pp.
- [64] W.S. Broecker, G.M. Henderson, The sequence of events surrounding Termination II and their implications for the cause of glacial-interglacial CO₂ changes, *Paleoceanography* 13 (1998) 352–364.
- [65] Z.R. Zhu, K.H. Wyrwoll, L.B. Collins, J.H. Chen, G.J. Wasserburg, A. Eisenhauer, High-precision U-series dating of Last Interglacial events by mass spectrometry: Houtman Abrolhos Islands, western Australia, *Earth Planet. Sci. Lett.* 118 (1993) 281–293.
- [66] C.H. Stirling, T.M. Esat, K. Lambeck, M.T. McCulloch, Timing of duration of the Last Interglacial: evidence for a restricted interval of widespread coral reef growth, *Earth Planet. Sci. Lett.* 160 (1998) 745–762.
- [67] M. Stein, G.J. Wasserburg, P. Aharon, J.H. Chen, Z.R. Zhu, A. Bloom, J. Chappell, TIMS U-series dating and stable isotopes of the last interglacial event in Papua New Guinea, *Geochim. Cosmochim. Acta* 57 (1993) 2541–2554.
- [68] T.M. Esat, M.T. McCulloch, J. Chappell, B. Pillans, A. Omura, Rapid fluctuations in sea level recorded at Huon Peninsula during the penultimate deglaciation, *Science* 283 (1999) 197–201.
- [69] E. Bard, C. Jouannic, B. Hamelin, P. Pirazzoli, M. Arnold, G. Faure, P. Sumosusastro, Syaefudin, Pleistocene sea levels at Sumba Island, Indonesia, *Geophys. Res. Lett.* 23 (1996) 1473–1476.
- [70] C. Lorius, J. Jouzel, C. Ritz, L. Merlivat, N.I. Barkov, Y.S. Korotkevitch, V.M. Kotlyakov, A 150,000-year climatic record from Antarctic ice, *Nature* 316 (1985) 591–596.
- [71] J.M. Barnola, P. Pimienta, D. Raynaud, Y.S. Korotkevich, CO₂-climate relationship as deduced from the Vostok ice core: A re-examination based on new measurements and on a re-evaluation of the air dating, *Tullus Series B* 43 (1991) 83–90.
- [72] K.R. Ludwig, K.R. Simmons, B.J. Szabo, I.J. Winograd, J.M. Landwehr, A.C. Riggs, R.L. Hoffman, Mass-spectrometric ²³⁰Th-²³⁴U-²³⁸U dating of the Devils Hole calcite vein, *Science* 258 (1992) 284–287.
- [73] I.J. Winograd, J.M. Landwehr, K.R. Ludwig, T.B. Coplen, A.C. Riggs, Duration and structure of the past four interglaciations, *Quat. Res.* 48 (1997) 141–154.
- [74] C. Gaven, C. Hillaire-Marcel, N. Petit-Maire, A Pleistocene lacustrine episode in south-eastern Libya, *Nature* 29 (1981) 131–133.
- [75] C. Causse, R. Coque, J.C. Fontes, F. Gasse, H. Ben Oueddou, K. Zouari, Two high levels of continental waters in the southern Tunisian chotts at about 90 and 150 ka, *Geology* 17 (1989) 922–925.
- [76] A.M. Lézine, J. Casanova, Correlated oceanic and continental records demonstrate past climate and hydrology of North Africa (0–140 ka), *Geology* 19 (1991) 307–310.
- [77] A.C. Clement, P. Seager, M.A. Cane, Orbital controls on the El Niño/Southern Oscillation and the tropical climate, *Paleoceanography* 14 (1999) 441–456.
- [78] A. Street-Perrott, Ancient tropical methane, *Nature* 366 (1993) 411–412.
- [79] Chappellaz, T. Blunier, D. Raynaud, J.M. Barnola, J. Schwander, B. Stauffer, Synchronous changes in atmospheric CH₄ and Greenland climate between 40 and 8 kyr BP, *Nature* 366 (1993) 443–445.
- [80] P.R. Renne, C.C. Swisher, A.L. Deino, D.B. Karner, T.L. Owens, D.J. DePaolo, Intercalibration of standards, absolute ages and uncertainties in ⁴⁰Ar/³⁹Ar dating, *Chem. Geol.* 145 (1998) 117–152.
- [81] I. McDougall, T.M. Harrison, *Geochronology and Thermochronology by the ⁴⁰Ar/³⁹Ar Method*, Oxford University Press, New York, 1988, 212 pp.
- [82] J.R. Taylor, *An Introduction to Error Analysis*, University Science Books, Mill Valley, CA, 1982.
- [83] S.D. Samson, E.C. Alexander Jr., Calibration of the interlaboratory ⁴⁰Ar/³⁹Ar dating standard, MMhb-1, *Chem. Geol. Isot. Geosci.* 66 (1988) 27–34.